Supplemental Material – Strain-controlled critical slowing down in the rheology of disordered networks

Jordan L. Shivers,[1,2,*] Abhinav Sharma,[3,4] and Fred C. MacKintosh[1,2,5,6]

[1]*Department of Chemical and Biomolecular Engineering, Rice University, Houston, TX 77005, USA*
[2]*Center for Theoretical Biological Physics, Rice University, Houston, TX 77005, USA*
[3]*Institute of Physics, University of Augsburg, 86159 Augsburg, Germany*
[4]*Leibniz-Institut für Polymerforschung Dresden, Institut Theorie der Polymere, 01069 Dresden, Germany*
[5]*Department of Chemistry, Rice University, Houston, TX 77005, USA*
[6]*Department of Physics & Astronomy, Rice University, Houston, TX 77005, USA*

CONTENTS

I. DISORDERED NETWORK MODEL

We consider the behavior of a bond-bending network [1] in a Newtonian solvent, in which drag forces act only on network nodes. We derive network structures with initial connectivity $z_0 \approx 6$ in 2D and $z_0 \approx 10$ in 3D from the contact networks of dense packings of soft spheres, which are generated using protocols described in prior work [2–4]. We then reduce the connectivity z to the desired value by selectively removing bonds randomly chosen from the set of nodes with the highest coordination number, yielding a network with a relatively homogeneous connectivity distribution [2]. The energy of the network is

$$U = \frac{\mu}{2}\sum_{ij}\frac{\left(\ell_{ij}-\ell_{ij,0}\right)^2}{\ell_{ij,0}} + \frac{\kappa}{2}\sum_{ijk}\frac{\left(\theta_{ijk}-\theta_{ijk,0}\right)^2}{\ell_{ijk,0}}$$

in which μ is the bond stretching stiffness (units of energy / length), κ is the bending rigidity (units of energy × length) acting between adjacent bonds, the instantaneous and rest lengths of bond ij are $\ell_{ij} = \mathbf{r}_j - \mathbf{r}_i$ and $\ell_{ij,0}$, the instantaneous and rest angle between bonds ij and jk are θ_{ijk} and $\theta_{ijk,0}$, and $\ell_{ijk,0} = (\ell_{ij,0} + \ell_{jk,0})/2$. We define the rest lengths and angles such that $U(\gamma_0 = 0) = 0$.

The node dynamics follow the over-damped, zero-temperature Langevin equation,

$$-\frac{\partial U}{\partial \mathbf{r}_i} - \zeta\left(\frac{d\mathbf{r}_i}{dt} - \mathbf{v}_f(\mathbf{r}_i)\right) = \mathbf{0}$$

in which ζ is the drag coefficient. Here, $\mathbf{v}_f(\mathbf{r}_i)$ denotes the velocity of the solvent at the position of node i. Note that we are using a free-draining [5] approximation and thus ignoring hydrodynamic interactions between nodes. We integrate this equation using the Euler method with timestep $\Delta t = 10^{-3}$. For convenience, we set $\mu = \zeta = 1$ and vary $\tilde{\kappa} = \kappa/(\mu\ell_0^2)$. Note that for $\tilde{\kappa} = 0$, the characteristic microscopic relaxation time is $\tau_0 = \zeta\ell_0/\mu$.

* Present affiliation: James Franck Institute and Department of Chemistry, University of Chicago, Chicago, Illinois 60637, USA

II. STRESS RELAXATION AT FINITE STRAIN

We first obtain the minimum energy configuration of the network at applied shear strain $\gamma = \gamma_0$ using the conjugate gradient method with a stopping criterion of $f_{\max} < 10^{-12}$, in which $f_{\max}$ is the magnitude of the largest net force on any node. Then, we apply a small, instantaneous *affine* shear strain step $\delta\gamma = 10^{-3}$, such that the strain becomes $\gamma = \gamma_0 + \delta\gamma$. Taking this as the initial state and assuming the solvent is immobile ($\mathbf{v}_f = \mathbf{0}$) in this case, we allow the system to evolve according to the equations of motion. We measure the shear stress $\sigma(t)$ as a function of time as the system evolves and compute the differential relaxation modulus,

$$K(\gamma_0, t) = \lim_{\delta\gamma \to 0} \frac{\sigma(\gamma_0 + \delta\gamma, t) - \sigma(\gamma_0, t \to \infty)}{\delta\gamma}$$

Note that $K_{\text{aff}}(\gamma_0) \equiv K(\gamma_0, t = 0)$ corresponds to the affine differential modulus, and the system eventually settles to the equilibrium (long-time) differential modulus $K_\infty(\gamma_0) \equiv K(\gamma_0, t \to \infty)$, equivalent to that measured under quasistatic shear.

III. SMALL-AMPLITUDE OSCILLATORY SHEAR AT FINITE STRAIN

For small-amplitude oscillatory shear near the critical strain, the system exhibits power-law scaling of the dynamic moduli over a range of frequencies bounded on the lower end by the critical characteristic frequency $\omega_c = |\gamma_0 - \gamma_c|^\phi$, governed by the proximity to the critical strain, and on the upper end by the characteristic frequency $\omega_0 \approx 1$ above which the network behaves as a solid. We assume that the ratio $\omega/\omega_c = \omega|\gamma_0 - \gamma_c|^{-\phi}$ governs the mechanics for a particular strain, in which case the differential modulus takes on the scaling form

$$K'(\omega) = |\gamma_0 - \gamma_c|^f \mathcal{H}_\pm \left(\omega|\gamma_0 - \gamma_c|^{-\phi}\right)$$

in which, for $x \gg 1$, $\mathcal{H}_-(c) \sim x^2$ and $\mathcal{H}_+(x) \sim$ constant, while for $x \gg 1$ we must have $\mathcal{H}_\pm(x) \propto x^{f/\phi}$ since $K'(\omega)$ remains finite.

Since at the critical strain we have $\delta\Gamma(\omega) \propto \omega^{-\lambda/\phi}$ and $K^*(\omega) \propto f/\phi$ (i.e. $\eta^*(\omega) \propto^{f/\phi - 1}$), the relation above implies $f/\phi - 1 = -\lambda/\phi$, or

$$f = \phi - \lambda$$

as we find for the stress relaxation case. Note that in Ref. [6], Yucht et al. made essentially the same argument relating the scaling behavior of the linear loss modulus and nonaffinity for networks near the isostatic point.

IV. POWER BALANCE

In the steadily oscillating regime (long after initiating the small-amplitude oscillatory shear), the power injected in the external application of strain, averaged over a single cycle, is

$$\begin{aligned} P_{\text{in}} &= V\frac{\omega}{2\pi}\int_{t_0}^{t_0+2\pi/\omega} \dot\gamma\left(\delta\sigma - \eta_f\dot\gamma\right)dt \\ &= V\frac{\omega}{2\pi}\int_{t_0}^{t_0+2\pi/\omega} \omega\delta\gamma\cos\omega t\left(\delta\gamma\left[K'\sin\omega t + K''\cos\omega t\right] - \eta_f\omega\delta\gamma\cos\omega t\right)dt \\ &= \frac{1}{2}V\omega\delta\gamma^2(K'' - \eta_f\omega) \end{aligned}$$

The nonaffine displacement of node i is $\mathbf{p}_i^{\text{NA}}(t) = \mathbf{u}_i^{\text{NA}}(\omega)\sin\left(\omega t + \theta^{\text{NA}}\right)$, and the nonaffine velocity is $\partial\mathbf{p}_i^{\text{NA}}/\partial t = \omega\mathbf{u}_i^{\text{NA}}(\omega)\cos\left(\omega t + \theta^{\text{NA}}\right)$. The system-wide instantaneous nonaffinity is $\delta\Gamma_i(\omega) = \sum_i \left\|\mathbf{u}_i^{\text{NA}}(\omega)\right\|^2 \sin^2(\omega t + \theta^{\text{NA}})/(\ell_0^2\delta\gamma^2)$. The power output, averaged over

a single cycle, in dragging the nodes against the solvent is

$$\begin{aligned}
P_{\text{out}} &= \sum_i \frac{\omega}{2\pi} \int_{t_0}^{t_0+2\pi/\omega} \mathbf{f}_{p,i} \cdot \left(\frac{\partial \mathbf{p}_i^{\text{NA}}}{\partial t} \right) dt \\
&= \sum_i \frac{\omega}{2\pi} \int_{t_0}^{t_0+2\pi/\omega} \zeta \left\| \frac{\partial \mathbf{p}_i^{\text{NA}}}{\partial t} \right\|^2 dt \\
&= \sum_i \frac{\omega}{2\pi} \int_{t_0}^{t_0+2\pi/\omega} \zeta \left\| \mathbf{u}_i^{\text{NA}}(\omega) \right\|^2 \omega^2 \cos^2(\omega t + \theta^{\text{NA}}) dt \\
&= \frac{1}{2} \zeta \omega^2 \sum_i \left\| \mathbf{u}_i^{\text{NA}}(\omega) \right\|^2 \\
&= \frac{1}{2} N \omega^2 \zeta \ell_0^2 \delta\gamma^2 \delta\Gamma(\omega)
\end{aligned}$$

Since $P_{\text{in}} = P_{\text{out}}$, we have

$$K''(\omega) - \eta_f \omega = \rho \omega \zeta \ell_0^2 \delta\Gamma(\omega)$$

in which $\rho = N/V$, hence

$$\eta'(\omega) - \eta_f = \rho \zeta \ell_0^2 \delta\Gamma(\omega)$$

For a quasistatic shear strain step $\delta\gamma$, the static nonaffinity, in terms of the individual static nonaffine displacements $\mathbf{u}_{i,\infty}^{\text{NA}}$, is

$$\delta\Gamma_\infty = \frac{1}{N \ell_0^2 \delta\gamma^2} \sum_i \| \mathbf{u}_{i,\infty}^{\text{NA}} \|^2$$

Note that since the static nonaffine displacement vector must be the same as the frequency-dependent nonaffine displacement vector in the zero-frequency limit, i.e. $\mathbf{u}_{i,\infty}^{\text{NA}} = \mathbf{u}_i^{\text{NA}}(\omega \to 0)$, we have $\delta\Gamma_\infty = \delta\Gamma(\omega \to 0)$. Thus, we can write the zero-shear viscosity $\eta_0 = \eta'(\omega \to 0)$ in terms of the static nonaffinity as

$$\eta_0 - \eta_f = \rho \zeta \ell_0^2 \delta\Gamma_\infty$$

V. RELAXATION TIME

We extract τ_c from the slope, on a log-linear plot, of the terminal exponential decay of $(\delta\sigma(t) - \delta\sigma_\infty)/\delta\sigma(0)$ vs t, as indicated in the inset for $\gamma_0 < \gamma_c$. Specifically, we calculate the slope of the final $n = 5$ points exceeding a sufficiently small threshold of $(\delta\sigma(t) - \delta\sigma_\infty)/\delta\sigma(0) = 10^{-6}$.

Another reasonable way of computing the relaxation time is (see Ref. [7])

$$\tau_c = \lim_{\omega \to 0} \frac{K'(\omega) - K_\infty}{\omega K''(\omega)} \equiv \lim_{\omega \to 0} \frac{\left(K'(\omega) - K_\infty\right)/\omega^2}{\eta'(\omega)}$$

which we can express in terms of $K(t)$. We can compute the dynamic moduli from the relaxation modulus as [8]

$$K'(\omega) = K_\infty + \omega \int_0^\infty \sin(\omega t) \left[K(t) - K_\infty\right] dt$$

and

$$K''(\omega) = \omega \int_0^\infty \cos(\omega t) \left[K(t) - K_\infty\right] dt$$

Thus

$$\lim_{\omega \to 0} \frac{K'(\omega) - K_\infty}{\omega^2} = \int_0^\infty t(K(t) - K_\infty) dt$$

and

$$\lim_{\omega\to 0} K''(\omega)/\omega = \int_0^\infty (K(t) - K_\infty)dt$$

Plugging these in, we find

$$\tau_c = \frac{\int_0^\infty t(K(t) - K_\infty)dt}{\int_0^\infty (K(t) - K_\infty)dt} = \frac{\int_0^\infty t(K(t) - K_\infty)dt}{\rho\zeta\ell_0^2\delta\Gamma_\infty}$$

In Fig. S1, we plot τ_c vs. $\gamma_c - \gamma$ for a spring network with $N = 6400$, $z = 3.5$, $\tilde{\kappa} = 0$ and $\delta\gamma = 10^{-4}$. The same data is plotted vs. γ_0 in Fig. 2b in the main text.

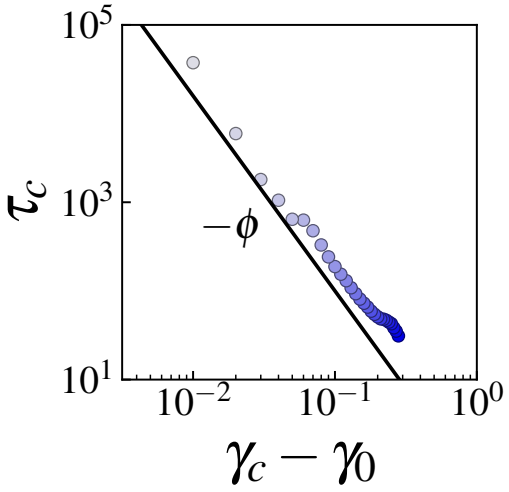

FIG. S1. Scaling of the slowest relaxation time τ_c with distance to the critical strain $\gamma_c - \gamma_0$, corresponding to the data presented in Fig. 2b in the main text. We observe excellent agreement with the predicted scaling $\tau_c \propto (\gamma_c - \gamma_0)^{-\phi}$ with $\phi = 2.2$.

VI. FINITE SIZE EFFECTS

We expect to observe the scaling relationships described in the main text when the correlation length is smaller than the system size. If τ_c diverges as $|\gamma_0 - \gamma_c|^{-\phi}$ in the $L \to \infty$ limit, then we expect

$$\tau_c \propto W^{\phi/\nu}\mathcal{A}(L^{1/\nu}(\gamma_0 - \gamma_c))$$

implying that we should observe $\tau_c(\gamma_c) \propto L^{\phi/\nu}$, a plot of $\tau_c L^{-\phi/\nu}$ vs. $L^{1/\nu}(\gamma_0 - \gamma_c)$ for varying L and γ_0 should yield a collapse. For the static differential nonaffinity, prior work has shown [4] $\delta\Gamma \propto L^{\lambda/\nu}\mathcal{B}(L^{1/\nu}(\gamma_0 - \gamma_c))$, so we expect the same finite-size scaling for the zero-shear viscosity,

$$\eta_0 - \eta_f \propto L^{\lambda/\nu}C(L^{1/\nu}(\gamma_0 - \gamma_c))$$

such that $\eta_0(\gamma_c) - \eta_f \propto L^{\lambda/\nu}$. Likewise, we should see a collapse of $(\eta_0 - \eta_f)L^{-\lambda/\nu}$ vs. $L^{1/\nu}(\gamma_0 - \gamma_c)$ for varying L and γ_0. Here, $\mathcal{A}$, $\mathcal{B}$, and C are scaling functions.

VII. NONAFFINITY AND VISCOSITY IN SOFT SPHERE SUSPENSIONS

We will now briefly explore the response of dense suspensions of frictionless soft spheres in two and three dimensions near the onset of rigidity (jamming). As noted in the main text, prior work [9] has pointed out a connection between the zero-shear viscosity and quasistatic nonaffine velocity fluctuations in suspensions under steady shear. To highlight the connection between

nonaffinity and viscosity we discussed in the main text (Eq. 2), we will demonstrate here that the static differential nonaffinity is equivalent to, and diverges as $\phi_0 \to \phi_j$ with the same exponent as, the excess viscosity.

These systems rigidify at a d-dimensional critical sphere volume fraction ϕ_j, with $\phi_{j,2D} \approx 0.84$ and $\phi_{j,3D} \approx 0.64$. Under steady shear conditions, dense suspensions at volume fractions below ϕ_j these have been shown to exhibit a zero-shear viscosity that scales with the volume (or area) fraction as $\eta_0 \propto (\phi_j - \phi_0)^{-\beta}$, in which β is an exponent generally reported in the range 2–2.8 in both simulations [10–15] and experiments [16, 17].

We consider N spheres with diameters split evenly between $d_i \in (d_0, 1.4d_0)$ to avoid crystallization [18]. The energy of a configuration with positions $\mathbf{r}_i$ is

$$U = \frac{\mu}{2} \sum_i \sum_{j>i} \left(1 - \|\mathbf{r}_j - \mathbf{r}_i\|/d_{ij}\right)^2 \Theta\left(1 - \|\mathbf{r}_j - \mathbf{r}_i\|/d_{ij}\right)$$

in which $d_{ij} = (d_i + d_j)/2$ and Φ is the Heaviside step function. To prepare initial configurations, we first randomly place the spheres in a d-dimensional box of side length $3L$ and quasistatically compress the system in small steps to a final side length L, chosen to yield the specified sphere volume fraction ϕ_0. Then, to produce a configuration consistent with slowly applied steady shear strain, we quasistatically apply (again in small steps) an initial simple shear of $\gamma_0 = 5$. Sample configurations are shown in Fig. S2.

Using the pre-sheared initial configuration, we follow the same stress relaxation procedure described earlier for networks, with $\delta\gamma = 10^{-5}$, and compute both the excess zero-shear viscosity $\eta_0 - \eta_f$ and static differential nonaffinity $\delta\Gamma_\infty$ as a function of volume fraction. For both $d = 2$ and $d = 3$, we observe values of the scaling exponent β consistent with the range reported in the literature (see Fig. S3a) and find that the relationship between zero-shear viscosity and static differential nonaffinity provided in Eq. 2 (main text), i.e. $\eta_0 - \eta_f = \rho\zeta\ell_0^2\delta\Gamma_\infty$, is consistently satisfied (see Fig. S3b). These results suggest that the static differential nonaffinity, which can be inexpensively computed by energy minimization after a single small shear strain step, could provide a complementary route for concretely determining the viscosity divergence exponent β in this and other related systems (e.g. suspensions of frictional spheres [19]). Note that a different viscosity divergence exponent $\beta \approx 1.5$ is observed for initial configurations generated without pre-shear [7]. Because the static differential nonaffinity necessarily scales with β irrespective of preparation, our results suggest that the distinction in scaling between isotropically compressed and pre-sheared suspensions is due to differences in their nonaffine response.

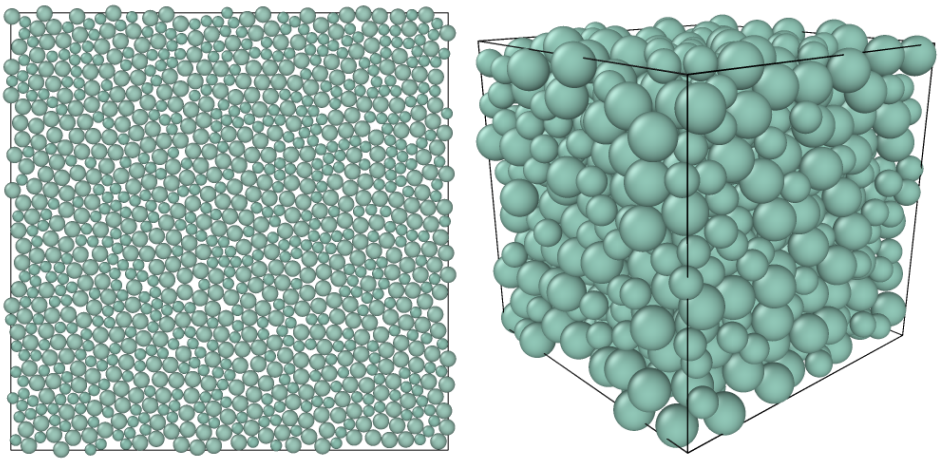

FIG. S2. (a) Radially bidisperse assemblies of $N = 1000$ spheres in (left) $d = 2$ with area fraction $\phi_0 = 0.84$ and (right) $d = 3$ with volume fraction $\phi_0 = 0.64$. Images prepared using Ovito [20].

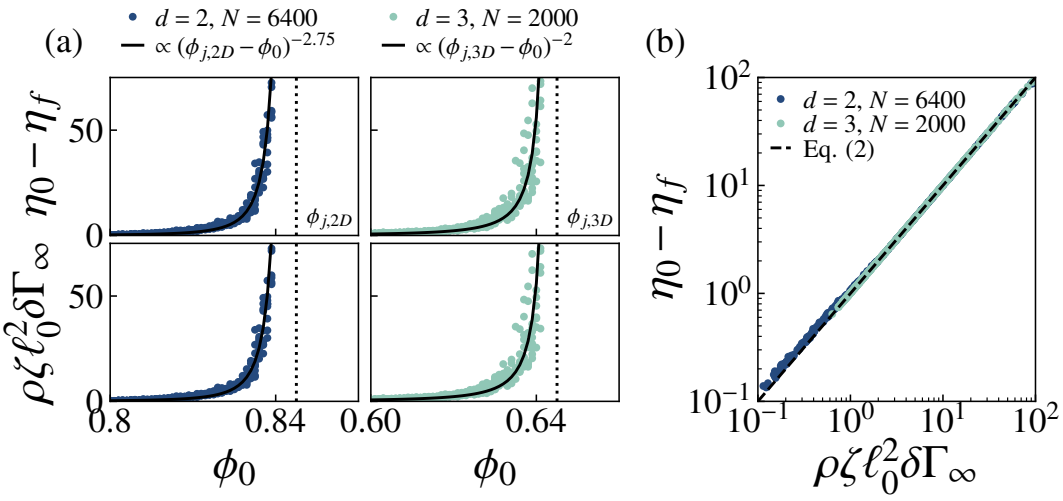

FIG. S3. (a) Excess zero-shear viscosity $\eta_0 - \eta_f$ and scaled static differential nonaffinity $\delta\Gamma_\infty$ for N spheres in two and three dimensions as a function of volume (or area) fraction ϕ_0, plotted with fits (solid lines) proportional to $(\phi_j - \phi_0)^{-\beta}$ as indicated above each column. Each point represents a measurement for a randomly generated sample, with 10 samples for each ϕ_0. Here, we use $\phi_{j,2D} = 0.845$ and $\phi_{j,3D} = 0.645$. (b) Eq. 2 (main text) is satisfied for both $d = 2$ and $d = 3$. Data are the same as in (a).

VIII. DEFINITION OF γ_c AND EXPANDED COLLAPSE PLOTS

For networks with $\tilde{\kappa} = 0$, we define the critical strain γ_c as the lowest value of the applied prestrain γ_0 at which the quasistatic differential shear modulus K_∞ is measurably nonzero, exceeding a cutoff of 10^{-6}. The precision of our determination of γ_c is thus limited by the spacing between γ_0 points, which we designate δ. The *true* value of the critical strain lies somewhere between our measured value γ_c and the previous strain point $\gamma_c - \delta$. Fig. S4a shows a zoomed-in view of the region of the plot of K_∞ vs. γ_0 provided in Fig. 2c in the main text.

To verify that our chosen spacing δ is sufficiently small, we check the dependence of the quality of the collapse plots in Fig. 2c (main text) on the chosen critical strain value. Let γ_c denote the critical strain defined in the main text, i.e. the first strain at which K_∞ is nonzero, and γ_c^* the critical strain value to be used in the collapse plots in Fig. S4. The black dotted line in Fig. S4 indicates the value used in the main text, $\gamma_c^* = \gamma_c$, while the red and blue dotted lines represent $\gamma_c^* = \gamma_c - \delta/3$ and $\gamma_c^* = \gamma_c - 2\delta/3$, respectively. Figs. S4b-d show the corresponding collapse plots. Note that Fig. S4b is simply an expanded version of Fig. 2c. We find that the quality of the collapse is insensitive to the choice of γ_c^*, suggesting that our chosen spacing δ is indeed sufficiently small.

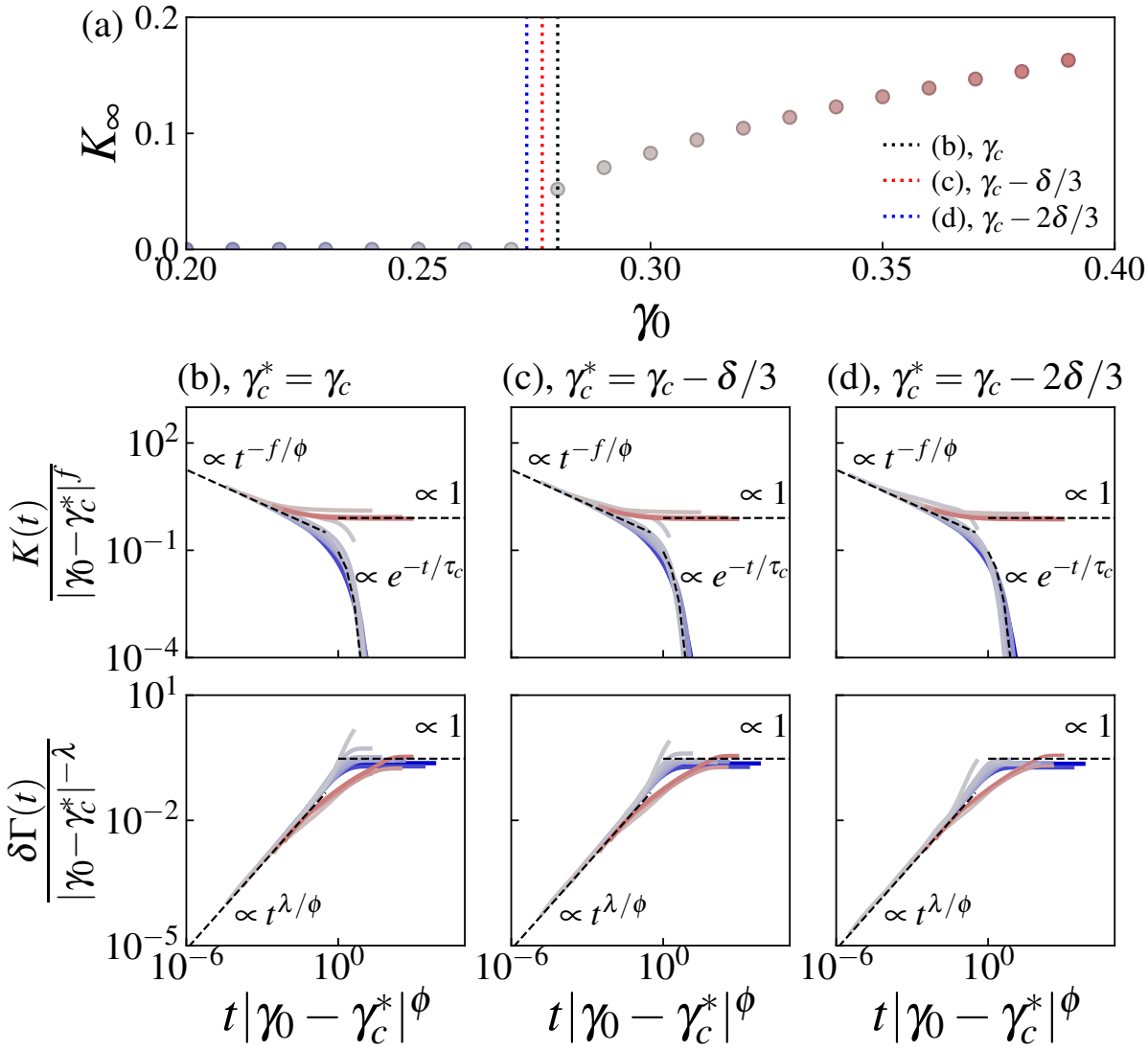

FIG. S4. (a) Quasistatic differential shear modulus K_∞ vs. prestrain γ_0, reproduced from Fig. 2b in the main text. The dotted lines represent possible values of the critical strain γ_c given the spacing δ between consecutive values of γ_0. The black dotted line represents the value of γ_c used in the main text, i.e. the first value of γ_0 at which the measured K_∞ is nonzero. Because the true value of γ_c is between $\gamma_c - \delta$ and γ_c, we can also consider other values in this range: the red and blue dotted lines correspond $\gamma_c - \delta/3$ and $\gamma_c - 2\delta/3$, respectively. (b-c) Reproducing the collapse plots of Fig. 2c (main text) using these values of γ_c^*, we observe little variation in the quality of the collapse, suggesting that the spacing δ is sufficiently small. Note that (b) is simply a reproduction of Fig. 2c in the main text.

[1] S. Arbabi and M. Sahimi, Physical Review B **38**, 7173 (1988).
[2] M. Wyart, H. Liang, A. Kabla, and L. Mahadevan, Physical Review Letters **101**, 215501 (2008).
[3] B. P. Tighe, Physical Review Letters **109**, 168303 (2012).
[4] J. L. Shivers, S. Arzash, A. Sharma, and F. C. MacKintosh, Physical Review Letters **122**, 188003 (2019).
[5] P. B. Visscher, P. Mitchell, and D. Heyes, Journal of Rheology **38**, 465 (1994).
[6] M. G. Yucht, M. Sheinman, and C. P. Broedersz, Soft Matter **9**, 7000 (2013).
[7] K. Saitoh, T. Hatano, A. Ikeda, and B. P. Tighe, Physical Review Letters **124**, 118001 (2020).
[8] J. D. Ferry, *Viscoelastic properties of polymers* (Wiley, New York, 1980), 3rd ed.
[9] B. Andreotti, J.-L. Barrat, and C. Heussinger, Physical Review Letters **109**, 105901 (2012).
[10] A. Ikeda, L. Berthier, and P. Sollich, Soft Matter **9**, 7669 (2013).
[11] T. Kawasaki, D. Coslovich, A. Ikeda, and L. Berthier, Physical Review E **91**, 012203 (2015).
[12] P. Olsson, Physical Review Letters **122**, 108003 (2019).

[13] A. Ikeda, T. Kawasaki, L. Berthier, K. Saitoh, and T. Hatano, Physical Review Letters **124**, 058001 (2020).
[14] Y. Nishikawa, A. Ikeda, and L. Berthier, Journal of Statistical Physics **182**, 37 (2021).
[15] M. Wang and J. F. Brady, Physical Review Letters **115**, 158301 (2015).
[16] F. Boyer, E. Guazzelli, and O. Pouliquen, Physical Review Letters **107**, 188301 (2011).
[17] W. B. Russel, N. J. Wagner, and J. Mewis, Journal of Rheology **57**, 1555 (2013).
[18] D. J. Koeze, D. Vågberg, B. B. Tjoa, and B. P. Tighe, Europhysics Letters **113**, 54001 (2016).
[19] A. Singh, C. Ness, R. Seto, J. J. de Pablo, and H. M. Jaeger, Physical Review Letters **124**, 248005 (2020).
[20] A. Stukowski, Modelling and Simulation in Materials Science and Engineering **18**, 015012 (2009).